

NACA RM L9G20

~~RESTRICTED~~  
CLASSIFICATION CHANGED

To UNCLASSIFIED

*W. L. Brydson per NACA  
release form 134  
By authority of 10/24/53*

~~RESTRICTED~~  
**NACA**



# RESEARCH MEMORANDUM

TWO-DIMENSIONAL WIND-TUNNEL INVESTIGATION OF  
A 6-PERCENT-THICK SYMMETRICAL CIRCULAR-ARC AIRFOIL  
SECTION WITH LEADING-EDGE AND TRAILING-EDGE  
HIGH-LIFT DEVICES DEFLECTED IN COMBINATION

By Robert J. Nuber and Gail A. Cheesman

Langley Aeronautical Laboratory  
Langley Air Force Base, Va.

CLASSIFIED DOCUMENT

This document contains classified information affecting the National Defense of the United States within the meaning of the Espionage Act, USC 50:33 and 32. Its transmission or the revelation of its contents in any manner to an unauthorized person is prohibited by law. Information so classified may be imparted only to persons in the military and naval services of the United States, appropriate civilian officers and employees of the Federal Government who have a legitimate interest therein, and to United States citizens of known loyalty and discretion who of necessity must be informed thereof.

**NATIONAL ADVISORY COMMITTEE  
FOR AERONAUTICS**

WASHINGTON

September 6, 1949

~~RESTRICTED~~

UNCLASSIFIED

NACA RM L9G20

NATIONAL ADVISORY COMMITTEE FOR AERONAUTICS

RESEARCH MEMORANDUM

TWO-DIMENSIONAL WIND-TUNNEL INVESTIGATION OF  
A 6-PERCENT-THICK SYMMETRICAL CIRCULAR-ARC AIRFOIL  
SECTION WITH LEADING-EDGE AND TRAILING-EDGE  
HIGH-LIFT DEVICES DEFLECTED IN COMBINATION  
By Robert J. Nuber and Gail A. Cheesman

SUMMARY

A two-dimensional wind-tunnel investigation was made of a 6-percent-thick symmetrical circular-arc airfoil with leading-edge and trailing-edge high-lift devices. The investigation was made to determine the effects on maximum section lift coefficient of different leading-edge slats and drooped-nose flaps of 15-percent chord when used in combination with a plain trailing-edge flap of 20-percent chord deflected  $60^\circ$ . Section lift characteristics of the airfoil with the various high-lift devices deflected in combination are presented for Reynolds numbers from  $0.7 \times 10^6$  to  $9.0 \times 10^6$ . Slat-position contours of maximum section lift coefficient and some pitching-moment characteristics are included.

The results indicated that a properly positioned leading-edge slat or a drooped-nose flap increased the maximum section lift coefficient of the airfoil with the plain trailing-edge flap deflected  $60^\circ$  from 1.63 to 2.02 or 1.96, respectively, and increased the angle of attack for maximum section lift coefficient from  $2.5^\circ$  to  $16^\circ$  or  $9^\circ$ , respectively. It was also found that varying the Reynolds number for either the slat or drooped-nose-flap configurations or moving the drooped-nose-flap hinge from the lower surface to the upper surface had essentially no effect on the lift characteristics.

INTRODUCTION

The use of wings with thin biconvex profiles for high-speed aircraft has necessitated the development of devices to increase the low

UNCLASSIFIED

maximum lift coefficients of these profiles in order that the airplane may fly satisfactorily in the low-speed range. Devices that have been suggested for this purpose are trailing-edge flaps, leading-edge flaps, and leading-edge slats. Of these devices, trailing-edge flaps and leading-edge flaps have been investigated. (See reference 1.)

The present paper gives the results of an investigation of a 6-percent-thick symmetrical circular-arc airfoil with a 15-percent-chord leading-edge slat deflected in combination with a 20-percent-chord plain trailing-edge flap having a  $60^\circ$  deflection. These results include the section lift characteristics, slat-position contours of maximum section lift coefficient, and some pitching-moment characteristics. Also included in the investigation are the effects on the section lift characteristics of varying the Reynolds number and of moving the hinge line from the lower surface to the upper surface of a 15-percent-chord leading-edge flap deflected  $27^\circ$  in combination with the 20-percent-chord plain trailing-edge flap having a deflection of  $60^\circ$ .

#### SYMBOLS

$c_l$  section lift coefficient  $\left( \frac{l}{q_0 c} \right)$

$c_{m_{c/4}}$  section pitching-moment coefficient about the quarter chord  
 $\left( \frac{m_{c/4}}{q_0 c^2} \right)$

where

$l$  lift per unit span

$m$  pitching moment per unit span

$c$  chord of airfoil with high-lift devices neutral

$q_0$  free-stream dynamic pressure  $\left( \frac{\rho_0 V_0^2}{2} \right)$

$\rho_0$  free-stream mass density

$V_0$  free-stream velocity

$\alpha_0$	section angle of attack, degrees
$c_{l_{max}}$	maximum section lift coefficient
$\Delta c_{l_{max}}$	increment of maximum section lift coefficient due to deflection of leading-edge high-lift devices
$\alpha_{c_{l_{max}}}$	section angle of attack at maximum lift coefficient
$\Delta \alpha_{c_{l_{max}}}$	increment of section angle of attack at maximum lift due to deflection of leading-edge high-lift devices
R	Reynolds number
$\delta_B$	angular deflection of leading-edge-slat chord line from airfoil chord line, positive when deflected below chord line, degrees
$\delta_N$	drooped-nose-flap deflection, positive when deflected below chord line, degrees
$\delta_F$	plain trailing-edge-flap deflection, positive when deflected below chord line, degrees
$x_B$	horizontal distance from reference point on main part of airfoil to the slat trailing edge, positive when slat moves forward, percent of airfoil chord
$y_B$	vertical distance from reference point on main part of airfoil to slat trailing edge, positive when slat moves upward, percent of airfoil chord

## MODEL

The model used in this investigation was a 24-inch-chord airfoil section built to a 6-percent-thick symmetrical circular-arc contour. Ordinates for this profile are presented in table I. The main part of the airfoil was made of steel. The 20-percent-chord plain trailing-edge flap, constructed of brass, was pivoted on leaf hinges mounted flush with the lower surface. (See reference 1.) The gap between the flap and flap skirt was sealed with modeling clay to prevent leakage. In all cases, the leading-edge slats and drooped-nose flaps were investigated in combination with the plain trailing-edge flap deflected 60°.

Slats.— The slats were constructed of brass and had chords equal to 15 percent of the airfoil chord. Ordinates and sketches of the three slat configurations tested are given in table II and figure 1, respectively.

Configurations 1 and 2 were designed so that, when the slats were retracted, they faired into the main part of the airfoil. For configuration 3, a small gap between the slat and main part of the airfoil existed on the lower surface with the slat neutral. Model end plates, as shown in figure 2, were used to facilitate changing the slat to any desired position. Slat end plates, which recessed into the model end plates, were used to change the slat deflection. The slat trailing-edge positions were measured from a reference point located on the upper surface of the main part of the airfoil at the 15-percent-chord station, as shown in figure 3. No intermediate supports were provided between the main part of the airfoil and the slat.

Drooped-nose flap.— The drooped-nose flaps were constructed of brass and had chords equal to 15 percent of the airfoil chord. For all tests, these flaps were deflected  $27^\circ$ . Configuration A was designed so that the drooped-nose flap pivoted on a leaf hinge-mounted flush with the lower surface, and the flap skirt was in rubbing contact with the flap. A sketch of this configuration is shown in figure 1. In order to determine the aerodynamic effects of changing the position of the hinge line, a lead bead was soldered to the upper surface of the flap and filed to a sharp corner. A sketch of this modification, designated configuration B, is also shown in figure 1.

## TESTS

The investigation was conducted in the Langley two-dimensional low-turbulence tunnel and the Langley two-dimensional low-turbulence pressure tunnel. A complete description of these wind tunnels, details of the test methods, and the methods used in correcting the data to free-air conditions are given in reference 2. All tests were made with the 20-percent-chord plain trailing-edge flap deflected  $60^\circ$  in combination with the leading-edge high-lift devices.

Slat.— Measurements were made at a Reynolds number of  $2.0 \times 10^6$  of the lift of the slat configurations to determine the ideal positions of the slats. The ideal position of the slat for a given deflection and slat configuration is defined as the position that yields the highest maximum section lift coefficient. For these tests, a wide horizontal and vertical range of slat locations was covered for several slat deflections and three slat configurations.

Section lift characteristics were determined for configuration 1 at a Reynolds number of  $2.0 \times 10^6$  for slat deflections of  $19.75^\circ$ ,  $25.5^\circ$ ,  $30^\circ$ , and  $35.25^\circ$ . Pitching moments were measured only for slat configuration 1 with the slat deflected  $25.5^\circ$  and  $30^\circ$ . The section lift characteristics of slat configuration 2 were determined at Reynolds numbers of  $2.0 \times 10^6$ ,  $6.0 \times 10^6$ , and  $9.0 \times 10^6$  with the slat deflected  $30^\circ$  and for configuration 3 at a Reynolds number of  $2.0 \times 10^6$  with the slat deflected  $30^\circ$ . Additional lift data for configurations 2 and 3 with the slats deflected  $35^\circ$  were obtained but are not included in this paper because the range of horizontal and vertical slat locations covered was insufficient to form a set of contours. These data, however, were found to be less favorable than those obtained with the slats deflected  $30^\circ$ .

Drooped-nose flap.— The lift characteristics were determined for drooped-nose-flap configuration A (hinge line on lower surface of drooped-nose flap) through a range of Reynolds numbers from  $0.70 \times 10^6$  to  $2.29 \times 10^6$ . The lift characteristics of configuration B (hinge line on upper surface of drooped-nose flap) were determined at Reynolds numbers of  $2.0 \times 10^6$  and  $6.0 \times 10^6$ .

## RESULTS AND DISCUSSION

Slat configurations.— Contours of maximum section lift coefficient obtained at a Reynolds number of  $2.0 \times 10^6$  are presented in figures 4, 5, and 6 for the three slat configurations at various slat positions and deflections. Maximum section lift coefficients and angles of attack for maximum lift coefficient at the ideal slat positions for given slat deflections are shown in these figures. The contours illustrate the sensitivity of the maximum section lift coefficient to changes in slat location for given slat deflections. Variation in slat trailing-edge height from the ideal position, particularly for an upward displacement, appears to be more critical, on the average, than chordwise variation.

The highest maximum section lift coefficients for each of the three slat configurations investigated occurred at a slat deflection of  $30^\circ$ .

The lift characteristics obtained at a Reynolds number of  $2.0 \times 10^6$  for slat configurations 1, 2, and 3 with the slats deflected  $30^\circ$  and located at their ideal positions are presented in figure 7. The magnitude of the maximum section lift coefficients varied from a value of 1.94 for configuration 2 to a value of 2.02 for configuration 3. It should be noted, however, that a small gap between the slat and the

airfoil exists on the lower surface of configuration 3 with the slat retracted. If such profile irregularities are to be avoided, particularly for supersonic flight, then configuration 1, which produces a maximum lift coefficient of 2.00, may be considered the most effective.

The section lift and pitching-moment characteristics of configuration 1, obtained at a Reynolds number of  $2.0 \times 10^6$  for the ideal positions of the slat for several slat deflections, are presented in figure 8. The maximum section lift coefficient for the  $25.5^\circ$  slat deflection is nearly equal to that obtained with a deflection of  $30^\circ$ . The aerodynamic center remains ahead of the quarter-chord point as shown by the section pitching-moment characteristics. For the  $30^\circ$  slat deflection, figure 8 shows that the magnitude and manner of variation of the moment coefficients are generally the same as those obtained with the drooped-nose flap deflected  $30^\circ$ .

The section lift characteristics of configuration 2, obtained at Reynolds numbers from  $2.0 \times 10^6$  to  $9.0 \times 10^6$  with the slat deflected  $30^\circ$ , are presented in figure 9. The maximum section lift coefficients are relatively unaffected by increases in the Reynolds number. Since no appreciable scale effect was obtained with configuration 2, it is believed that the effects of Reynolds number variations on  $c_{l_{\max}}$  for configurations 1 and 3 also may be considered negligible.

Drooped-nose-flap configurations.— The section lift characteristics of configuration A are presented in figure 10 for Reynolds numbers from  $0.70 \times 10^6$  to  $2.29 \times 10^6$ . It is seen in figure 10 that the maximum section lift characteristics remain practically constant with increasing Reynolds number. These results conform, in this respect, with the data presented in references 1 and 3 for the 6- and 7.5-percent-thick circular-arc airfoils with corresponding flap deflections.

The section lift characteristics of configuration B are presented in figure 11 for Reynolds numbers of  $2.0 \times 10^6$  and  $6.0 \times 10^6$ . Included in the figure for comparison are the section lift characteristics of configuration A corresponding to a Reynolds number of  $2.0 \times 10^6$ . The lift characteristics were practically unaffected when the hinge line of the drooped-nose flap was moved from the lower surface to the upper surface or when the Reynolds number of configuration B was increased from  $2.0 \times 10^6$  to  $6.0 \times 10^6$ .

It may be noted that the lift curves for configuration A at a Reynolds number of  $1.98 \times 10^6$  (fig. 10) and at a Reynolds number of  $2.0 \times 10^6$  (fig. 11) are not quite in agreement near maximum lift.

The discrepancies are not considered important and may be attributed to the fact that the two runs were made in different tunnels with a time interval of about 2 years between tests.

The maximum section lift coefficient of the airfoil with the plain trailing-edge flap deflected  $60^\circ$  (reference 1) is increased from a value of 1.63 to 1.96, and the angle of attack for maximum section lift coefficient is increased from  $2.5^\circ$  to  $9^\circ$  when the drooped nose is deflected  $27^\circ$  (configuration B).

Comparison of slat and drooped-nose-flap configurations.— Increments of maximum section lift coefficient  $\Delta c_{l_{\max}}$  and increments of section angle of attack for maximum lift coefficient  $\Delta \alpha_{c_{l_{\max}}}$  that result from deflection of the slat or drooped-nose flap are summarized graphically in figure 12. Included in the figure are comparative data taken from reference 1 ( $R = 6.0 \times 10^6$ ) for several deflections of the drooped-nose flap. The increments in maximum section lift coefficient for slat configuration 1 over a large range of deflections are greater than those obtained with the drooped-nose flap. Increments in angle of attack for maximum section lift coefficient are greater for the slats than for the drooped-nose flaps but the lift-curve peaks are similar. The differences in maximum section lift coefficient can be attributed, in part, to the greater projected area of the slat configurations. It must be emphasized, however, that, although slat configurations 1 and 3 are slightly more effective than the other leading-edge high-lift devices investigated, the drooped-nose-flap configurations may be more attractive to the designer in view of the structural and mechanical problems presented by slatted airfoils and because of the sensitivity of the maximum section lift coefficients of slatted airfoils to slat-position changes resulting from air loads and manufacturing irregularities.

It is believed that the air loads on the slats may be substantially equivalent to the air loads on the drooped-nose flap (reference 4) for corresponding deflections because the peak pressures near the leading edge of both types of high-lift devices are limited by separation.

Table III presents a summary of the highest maximum section lift coefficients, the angles of attack at which the maximum section lift coefficients occurred, and the increments that were obtained for the slat and drooped-nose-flap configurations investigated at a Reynolds number of  $2.0 \times 10^6$ . Also included in table III are the maximum section lift coefficients and angles of attack for maximum lift coefficient obtained at a Reynolds number of  $6.0 \times 10^6$  for the plain airfoil and the airfoil with the plain trailing-edge flap deflected  $60^\circ$  (reference 1).



## CONCLUSIONS

The results of a two-dimensional wind-tunnel investigation at Reynolds numbers from  $0.70 \times 10^6$  to  $9.0 \times 10^6$  of a 6-percent-thick symmetrical circular-arc airfoil with either a 15-percent-chord leading-edge slat or a 15-percent-chord drooped-nose flap and a 20-percent-chord plain trailing-edge flap deflected  $60^\circ$  indicated the following conclusions:

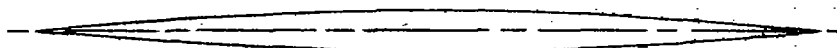
1. A properly positioned leading-edge slat or a drooped-nose flap increased the maximum section lift coefficient of the airfoil with the plain trailing-edge flap deflected  $60^\circ$  from a value of 1.63 to 2.02 or 1.96, respectively, and increased the angle of attack for maximum section lift coefficient from  $2.5^\circ$  to  $16^\circ$  or  $9^\circ$ , respectively.
2. The maximum section lift characteristics of the slat configurations are extremely sensitive to changes from the ideal slat position.
3. The type of lift-curve peak and the magnitude and manner of variation of the pitching-moment coefficients of the slat and drooped-nose-flap configurations are similar for a deflection of  $30^\circ$ .
4. The maximum section lift characteristics of the slat and drooped-nose-flap configurations tested are relatively unaffected by variations of Reynolds number.
5. Moving the position of the drooped-nose-flap hinge from the lower surface to the upper surface had practically no effect on the lift characteristics.

Langley Aeronautical Laboratory  
National Advisory Committee for Aeronautics  
Langley Air Force Base, Va.

## REFERENCES

1. Underwood, William J., and Nuber, Robert J.: Two-Dimensional Wind-Tunnel Investigation at High Reynolds Numbers of Two Symmetrical Circular-Arc Airfoil Sections with High-Lift Devices. NACA RM L6K22, 1947.
2. Von Doenhoff, Albert E., and Abbott, Frank T., Jr.: The Langley Two-Dimensional Low-Turbulence Pressure Tunnel. NACA TN 1283, 1947.
3. Powter, G. J., and Young, A. D.: Wind Tunnel Tests on a 7.5-Percent-Thick Bi-Convex Wing with Leading and Trailing Edge Flaps. R.A.E. Rep. No. Aero. 2157, British R.A.E., Sept. 1946.
4. Underwood, William J., and Nuber, Robert J.: Aerodynamic Load Measurements over Leading-Edge and Trailing-Edge Plain Flaps on a 6-Percent-Thick Symmetrical Circular-Arc Airfoil Section. NACA RM L7H04, 1947.

TABLE I  
ORDINATES FOR THE PLAIN AIRFOIL  
[Stations and ordinates given  
in percent of airfoil chord]

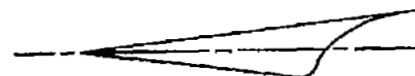
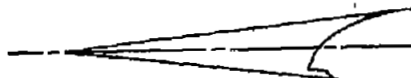
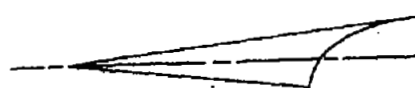


6-percent-thick symmetrical circular-arc airfoil			
Upper surface		Lower surface	
Station	Ordinate	Station	Ordinate
0	0	0	0
5	.572	5	-.572
10	1.082	10	-1.082
15	1.533	15	-1.533
20	1.922	20	-1.922
25	2.252	25	-2.252
30	2.521	30	-2.521
35	2.731	35	-2.731
40	2.880	40	-2.880
45	2.970	45	-2.970
50	3.000	50	-3.000
55	2.970	55	-2.970
60	2.880	60	-2.880
65	2.731	65	-2.731
70	2.521	70	-2.521
75	2.252	75	-2.252
80	1.922	80	-1.922
85	1.533	85	-1.533
90	1.082	90	-1.082
95	.572	95	-.572
100	0	100	0



TABLE II  
LEADING-EDGE SLAT AND MAIN AIRFOIL NOSE ORDINATES  
[Station and ordinates given in percent of airfoil chord]

LEADING-EDGE SLAT



CONFIGURATION 1			
Upper surface		Lower surface	
Station	Ordinate	Station	Ordinate
0	0	0	0
.500	.060	.500	-.060
.750	.090	.750	-.090
1.250	.149	1.250	-.149
2.500	.293	2.500	-.293
5.000	.572	5.000	-.572
7.500	.835	7.500	-.835
10.000	1.082	10.000	-1.082
15.000	1.533	10.458	-1.133
		10.667	-.492
		10.833	-.204
		11.250	.254
		12.083	.821
		12.917	1.150
		13.750	1.350
		15.000	1.533

CONFIGURATION 2			
Upper surface		Lower surface	
Station	Ordinate	Station	Ordinate
0	0	0	0
.500	.060	.500	-.060
.750	.090	.750	-.090
1.250	.149	1.250	-.149
2.500	.293	2.500	-.293
5.000	.572	5.000	-.572
7.500	.835	7.500	-.835
10.000	1.082	10.000	-1.082
15.000	1.533	11.875	-1.258
		11.417	-1.163
		11.083	-.933
		10.504	-.867
		10.667	-.492
		10.833	-.204
		11.250	.254
		12.083	.821
		12.917	1.150
		13.750	1.350
		15.000	1.533

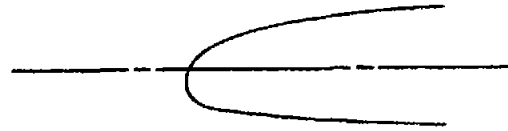
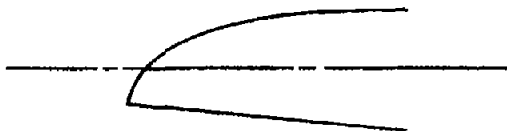
CONFIGURATION 3			
Upper surface		Lower surface	
Station	Ordinate	Station	Ordinate
0	0	0	0
.500	.060	.500	-.060
.750	.090	.750	-.090
1.250	.149	1.250	-.149
2.500	.293	2.500	-.293
5.000	.572	5.000	-.572
7.500	.835	7.500	-.835
10.000	1.082	10.000	-1.082
15.000	1.533	10.250	-1.042
		10.417	-.929
		10.583	-.650
		10.667	-.492
		10.833	-.204
		11.250	.254
		12.083	.821
		12.917	1.150
		13.750	1.350
		15.000	1.533



TABLE II - Concluded

LEADING-EDGE SLAT AND MAIN AIRFOIL NOSE ORDINATES - Concluded

## MAIN AIRFOIL NOSE



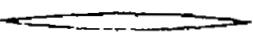
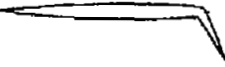
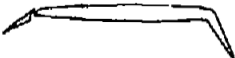
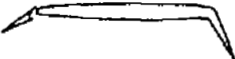
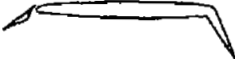
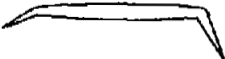
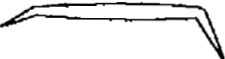
CONFIGURATION 1			
Upper surface		Lower surface	
Station	Ordinate	Station	Ordinate
10.458	-1.133	10.458	-1.133
10.667	-.512	11.250	-1.204
10.833	-.225	12.917	-1.354
11.250	.233	15.000	-1.533
12.083	.808	16.667	-1.667
12.917	1.142	18.333	-1.792
13.750	1.346	20.000	-1.922
15.000	1.533		
16.667	1.667		
18.333	1.792		
20.000	1.922		

CONFIGURATIONS 2 and 3			
Upper surface		Lower surface	
Station	Ordinate	Station	Ordinate
11.000	-.417	11.000	-.417
11.167	.079	11.167	-.917
11.333	.283	11.333	-1.079
11.500	.425	11.500	-1.175
11.667	.550	11.667	-1.233
12.083	.808	11.875	-1.258
12.917	1.142	12.083	-1.283
13.750	1.346	12.917	-1.354
15.000	1.533	15.000	-1.533
16.667	1.667	16.667	-1.667
18.333	1.792	18.333	-1.792
20.000	1.922	20.000	-1.922
L.E. radius: 0.833 $x = 11.833$ $y = -0.417$			

NACA

TABLE III

SUMMARY OF MAXIMUM-LIFT CHARACTERISTICS FOR LEADING-EDGE SLAT AND DROOPED-NOSE FLAP CONFIGURATIONS FOR THE  
NACA 28-(50)(03)-(50)(03) AIRFOIL

Profile	Config- uration	$c_{l_{max}}$	$\alpha_{c_{l_{max}}}$ (deg)	$\Delta c_{l_{max}}$	$\Delta \alpha_{c_{l_{max}}}$	$x_B$ (percent chord)	$y_B$ (percent chord)	gap (percent chord)	$\delta_n$ or $\delta_N$ (deg)	$\delta_F$ (deg)	R	Figure
		.73	8	—	—	—	—	—	—	—	$6 \times 10^6$	4(a) of reference 1
		1.63	2.5	0	0	—	—	—	—	60	6	5(a) of reference 1
	1	2.00	14	.37	11.5	4.23	-.26	1.06	30	60	2	7
	2	1.94	14	.31	11.5	3.81	-.26	.82	30	60	2	7
	3	2.02	16	.39	13.5	4.23	.52	1.73	30	60	2	7
	A	1.95	9	.32	6.5	—	—	—	27	60	2	11
	B	1.96	9	.33	6.5	—	—	—	27	60	2	11



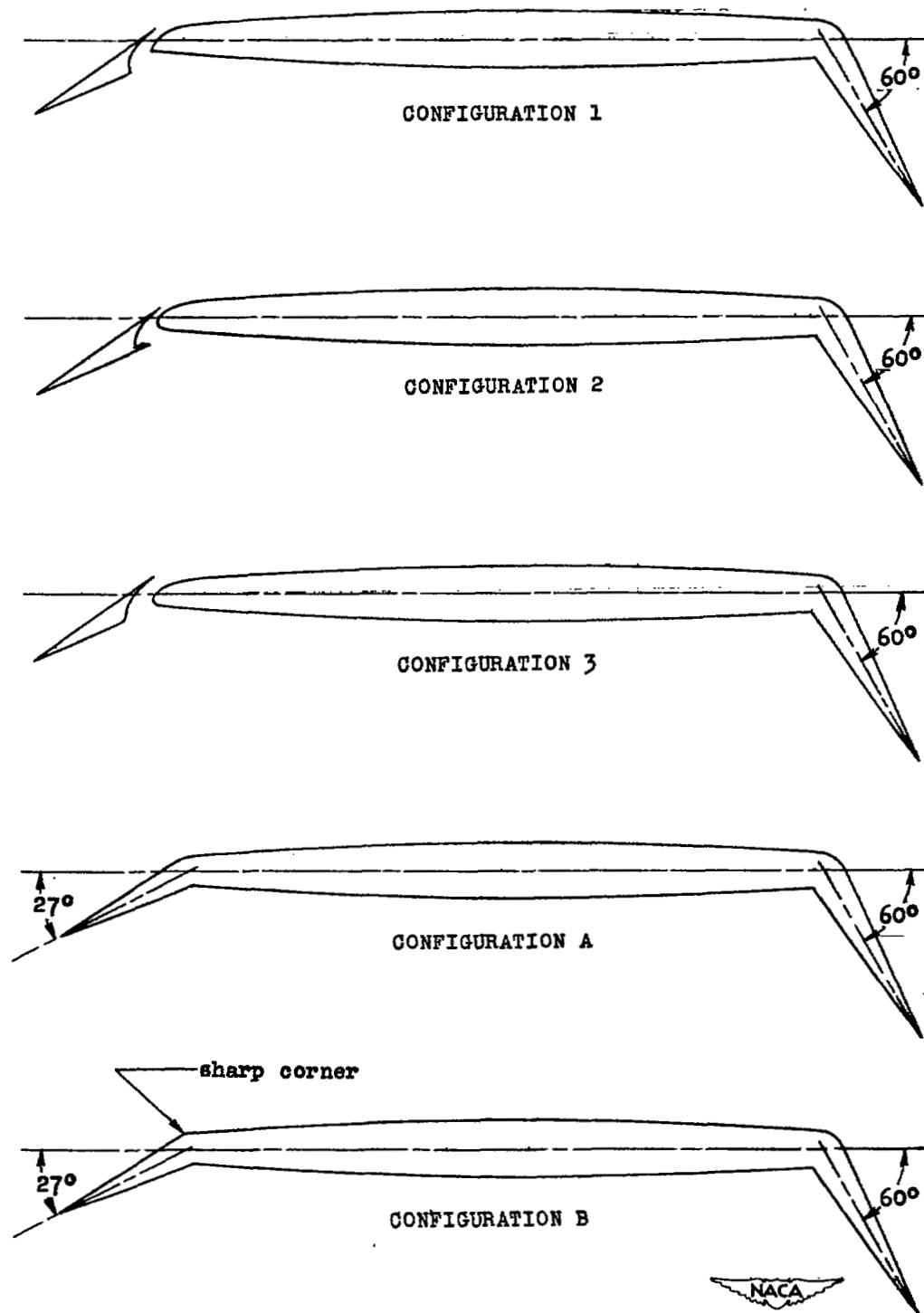


Figure 1.- Symmetrical circular-arc airfoil with leading-edge and trailing-edge high-lift devices.



Figure 2.- Model end plate used with slat configurations.





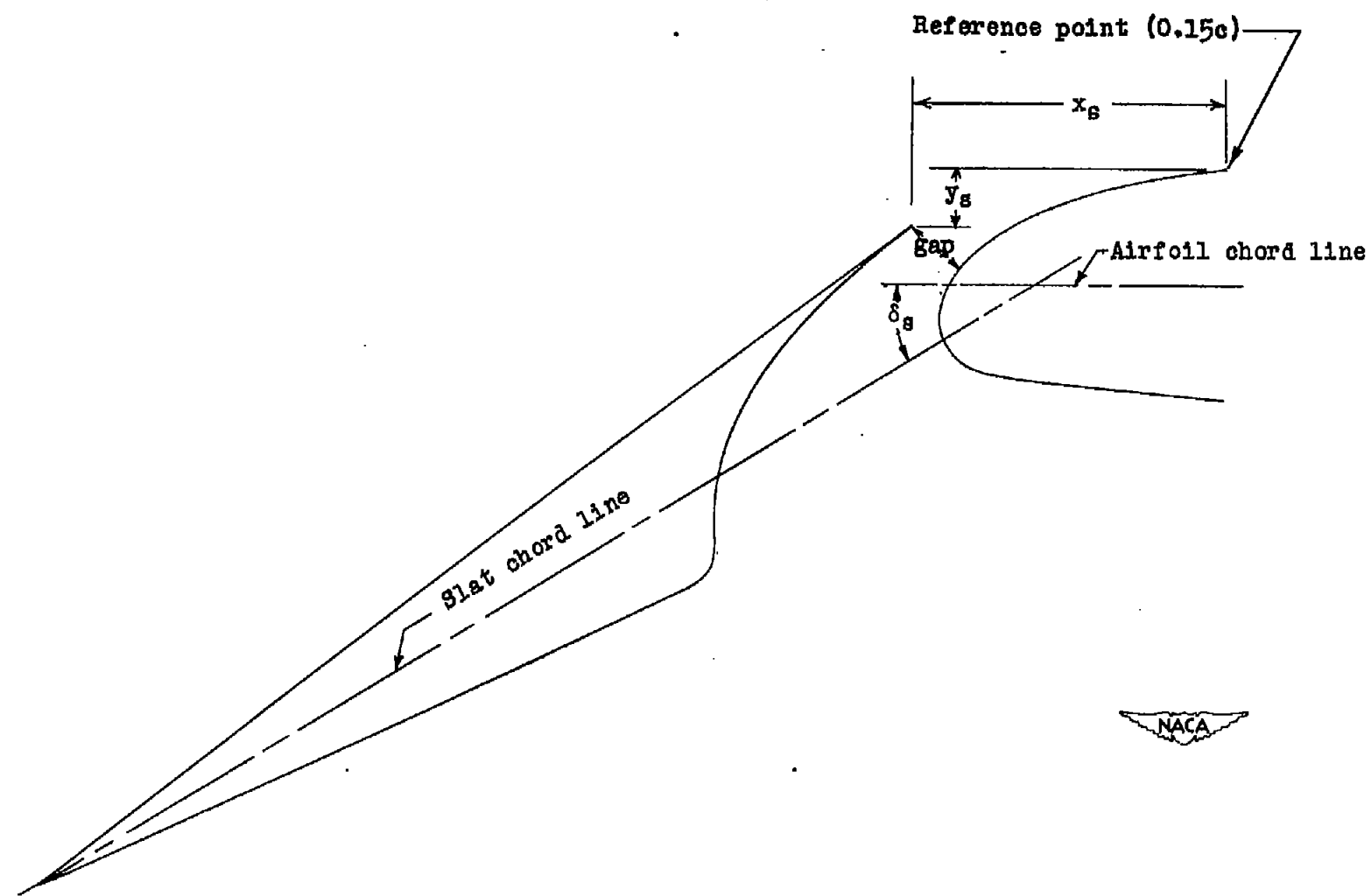
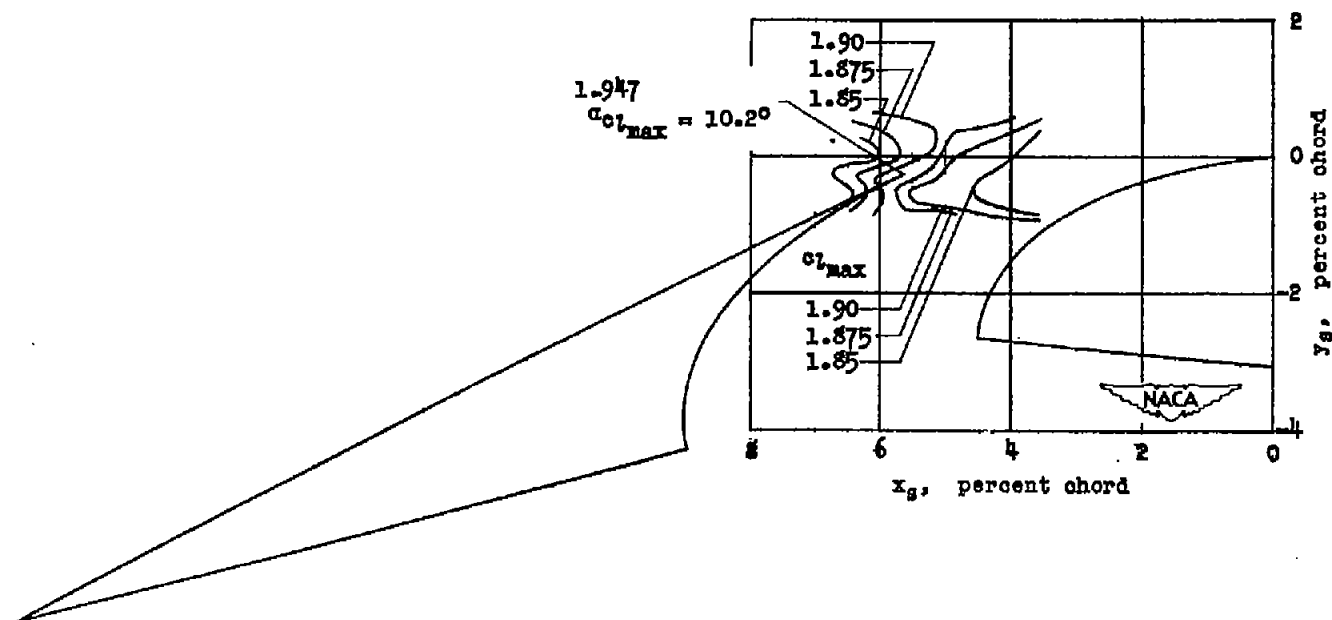
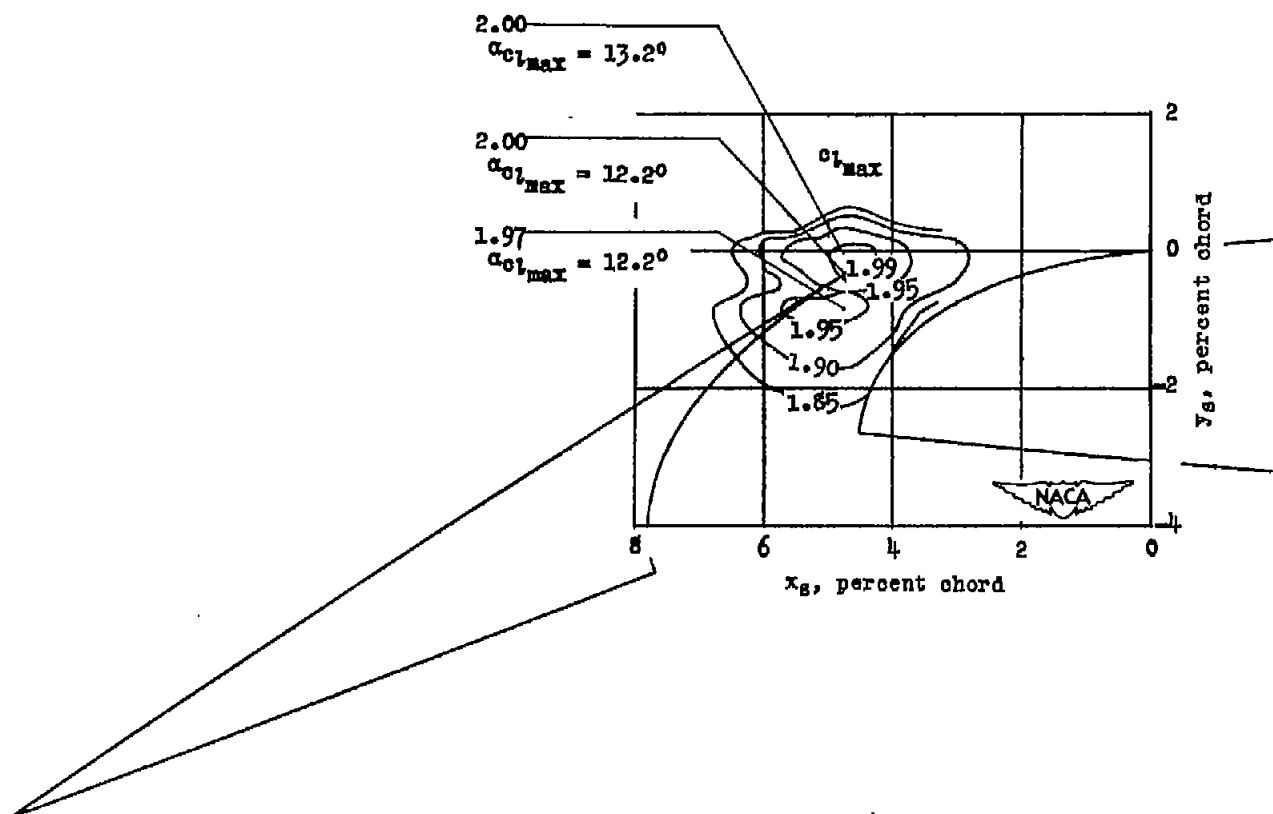


Figure 3.- Variables used to indicate position of leading-edge slat.



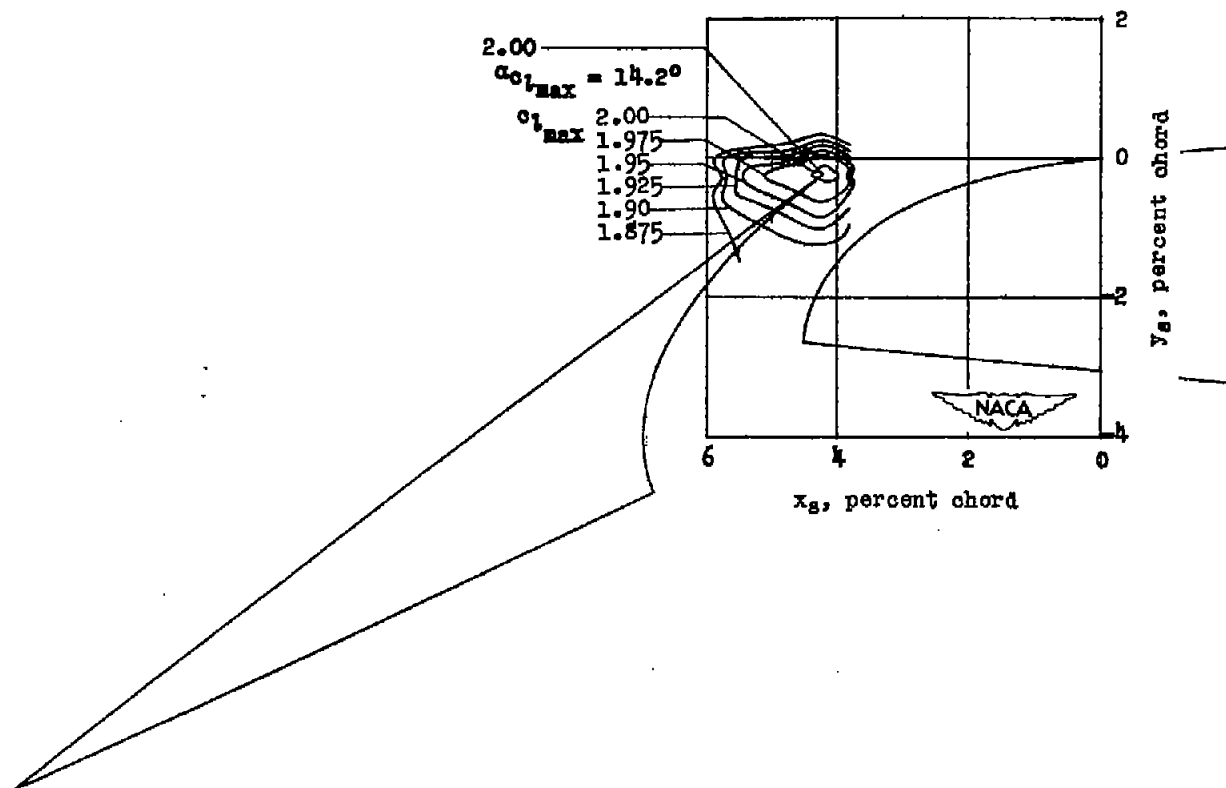
(a)  $\delta_B = 19.75^\circ$ .

Figure 4.- ~~Contours of maximum~~ <sup>Contours of maximum</sup> section lift coefficient for various positions of a 0.15c leading-edge slat on a 6-percent-thick symmetrical circular-arc airfoil. Configuration 1;  $R = 2 \times 10^6$ .



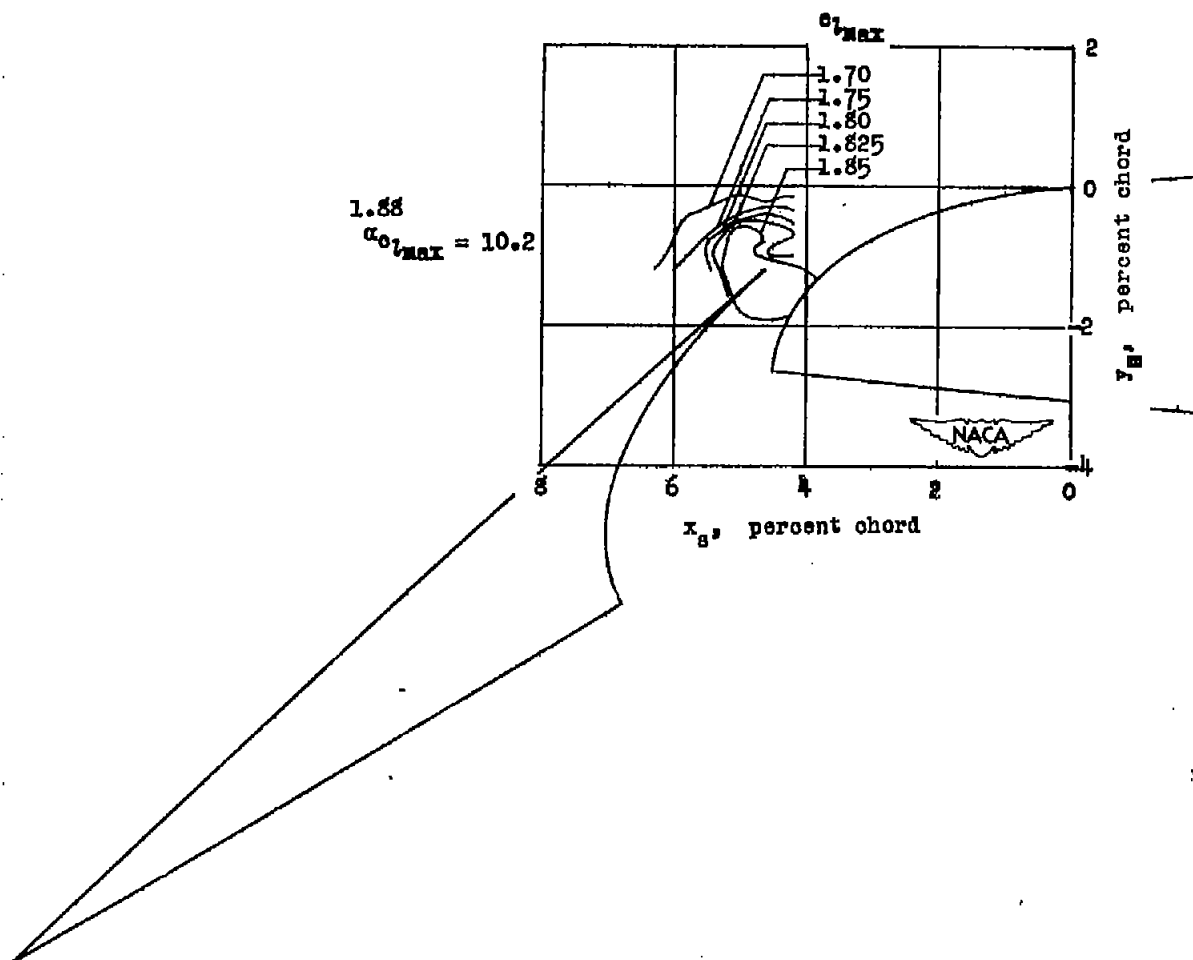
(b)  $\delta_B = 25.5^\circ$ .

Figure 4.- Continued.



(c)  $\delta_B = 30^\circ$ .

Figure 4.- Continued.



(d)  $\delta_B = 35.25^\circ$ .

Figure 4.- Concluded.

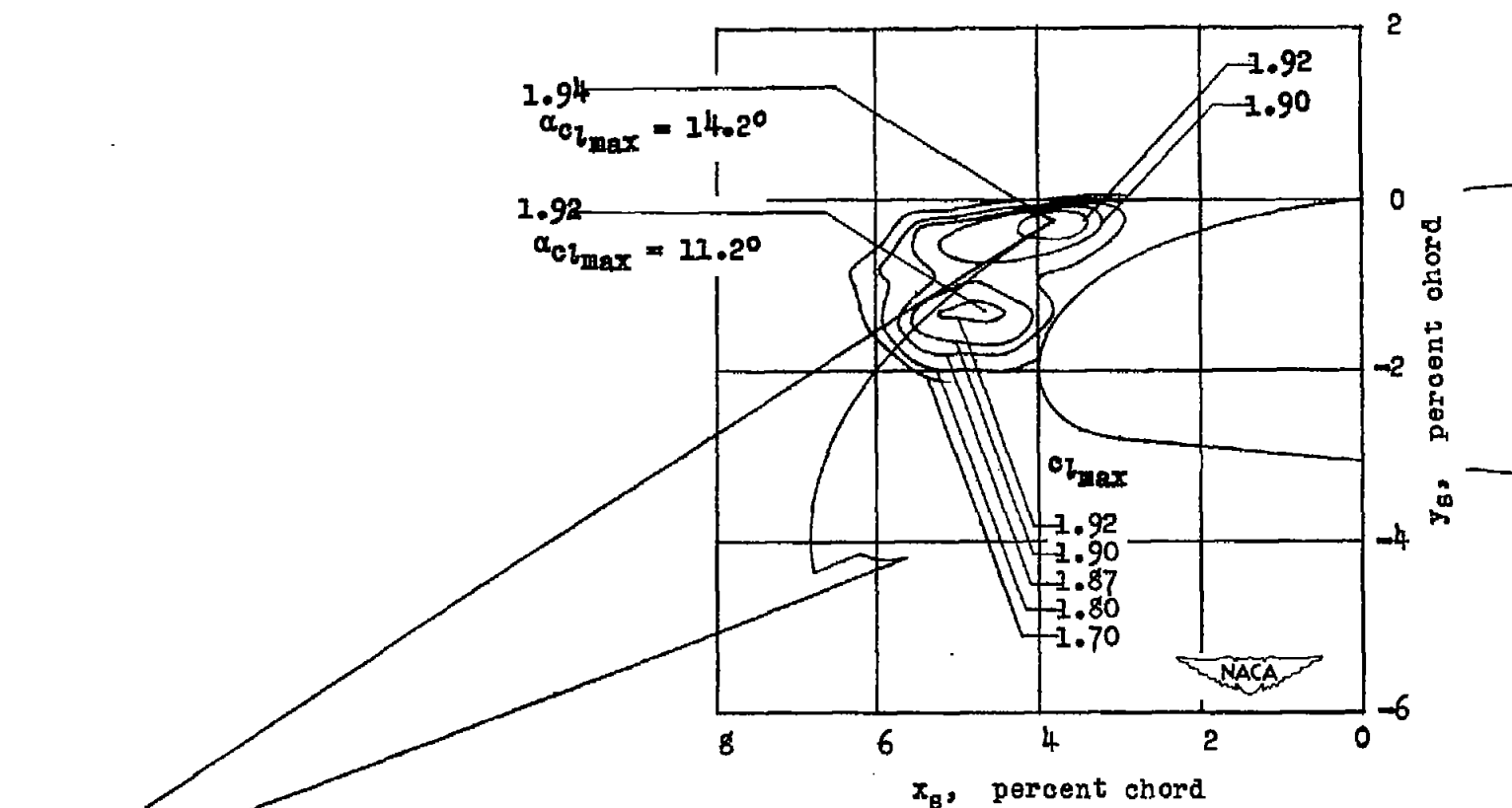
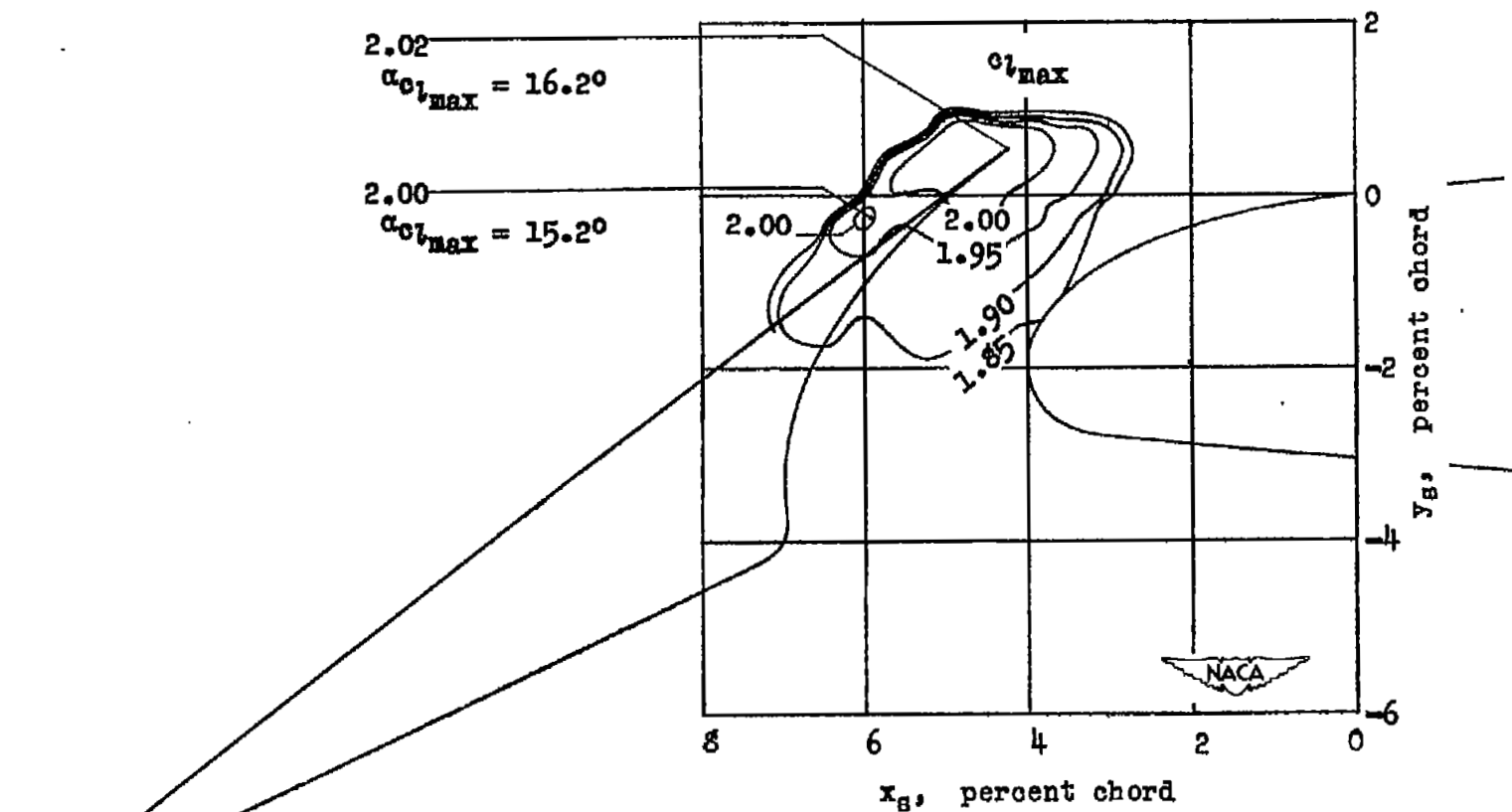


Figure 5.- ~~Contours of~~ maximum section lift coefficient for various positions of the 0.15c leading-edge slot on a 6-percent-thick symmetrical circular-arc airfoil. Configuration 2;  $\delta_s = 30^\circ$ ;  $R = 2 \times 10^6$ .



locus of t.e. of slat for  
 Figure 6.- Contours of maximum section lift coefficient for various positions of the 0.15c leading-edge  
 slat on a 6-percent-thick symmetrical circular-arc airfoil. Configuration 3;  $\delta_B = 30^\circ$ ;  
 $R = 2 \times 10^6$ .



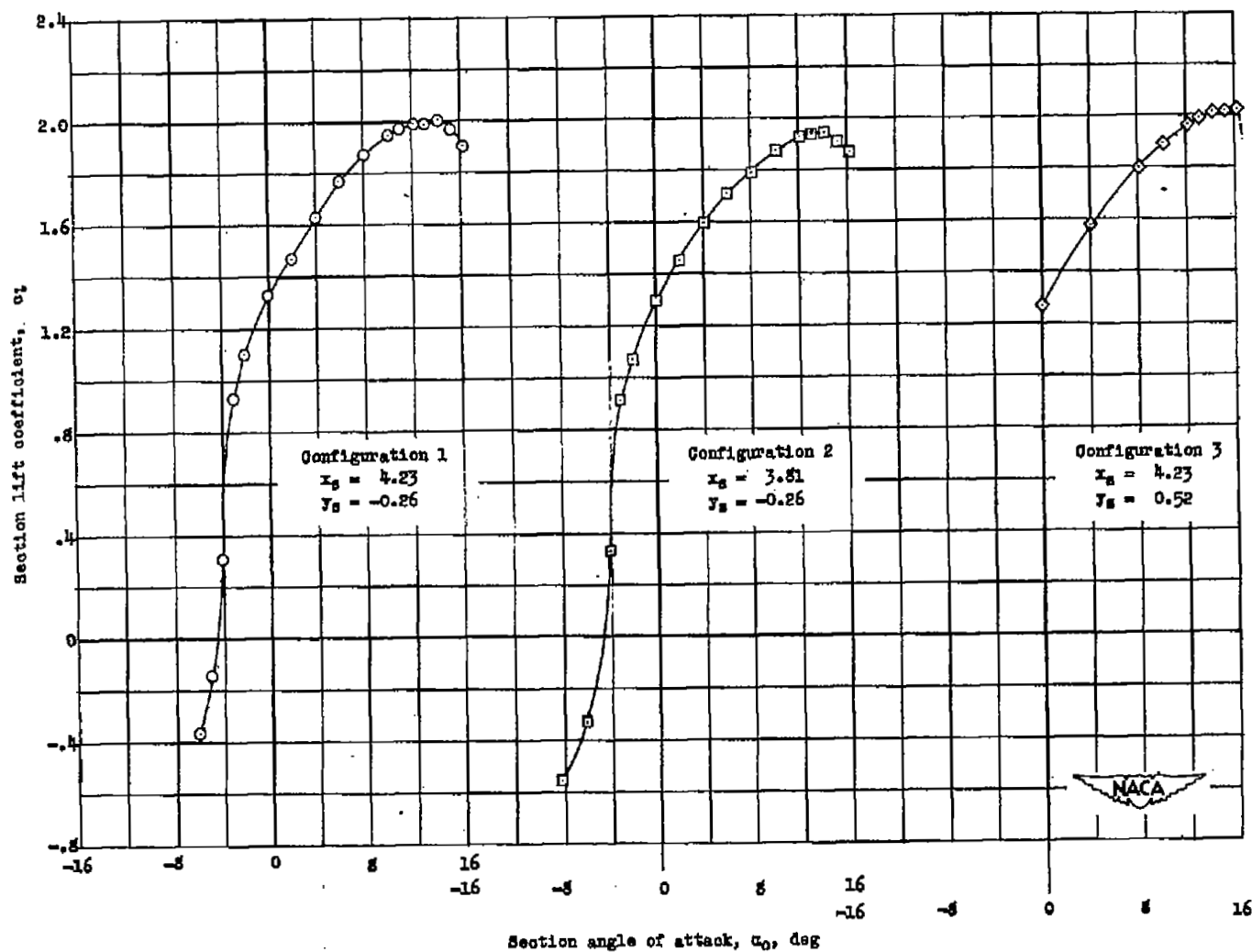


Figure 7.- Section lift characteristics of 6-percent-thick symmetrical circular-arc airfoil for various slat configurations.  $\delta_s = 30^\circ$ ;  $R = 2 \times 10^6$ .

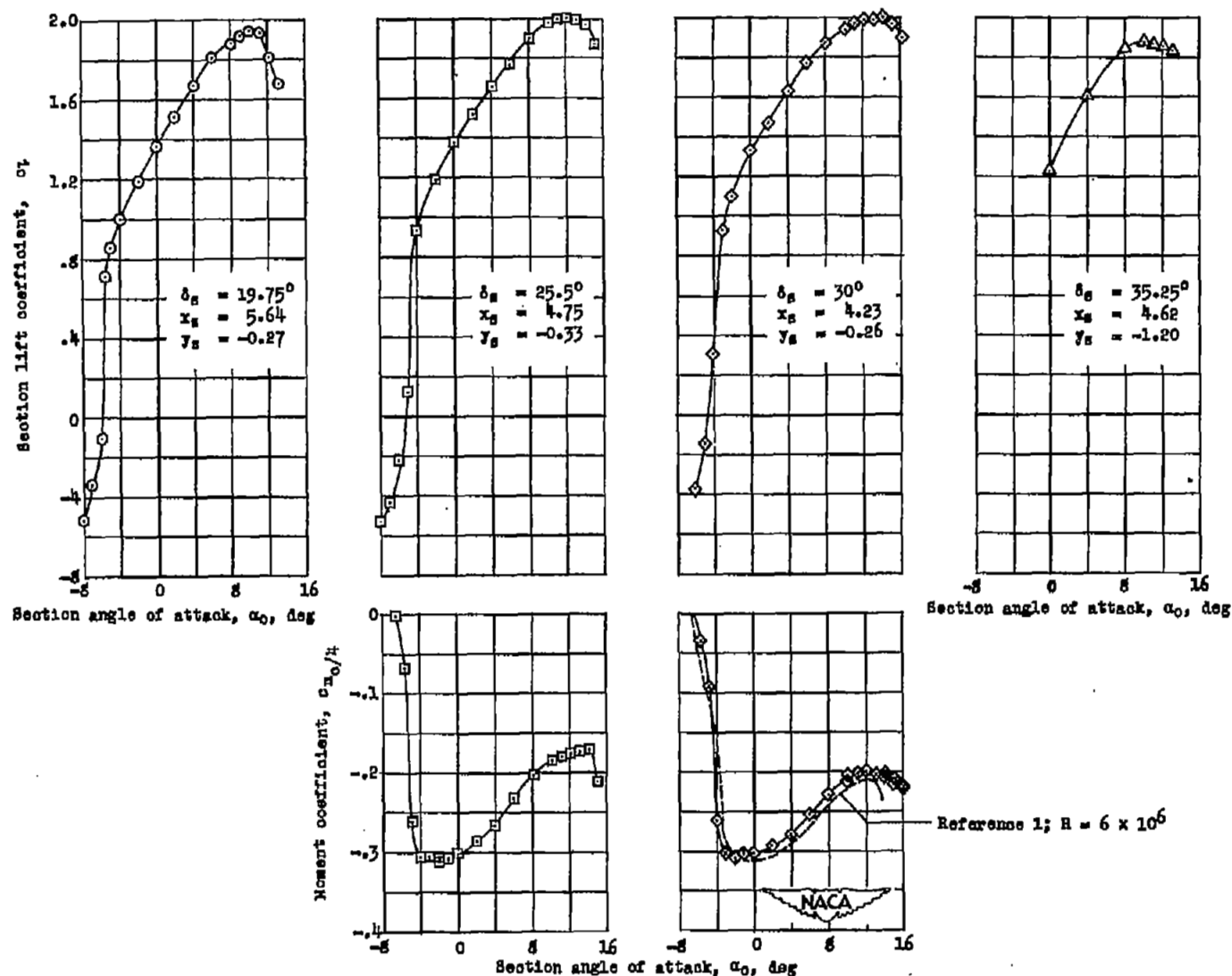


Figure 8.- Section lift and pitching-moment characteristics of 6-percent-thick symmetrical circular-arc airfoil for various deflections of the leading-edge slat. Configuration 1;  $R = 2 \times 10^6$ .

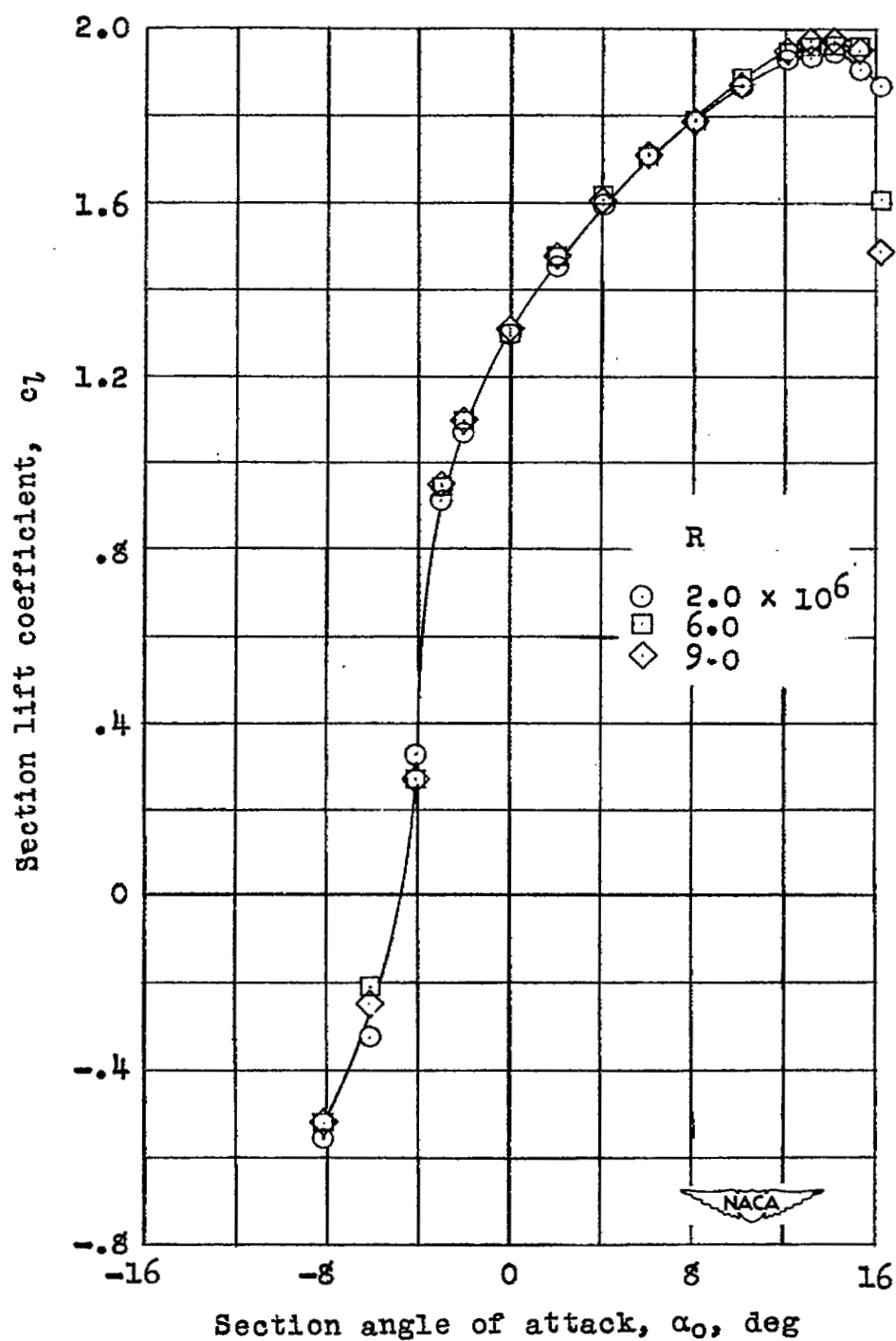


Figure 9.- Section lift characteristics at three values of the Reynolds number for 6-percent-thick symmetrical circular-arc airfoil with leading-edge slat. Configuration 2;  $\delta_s = 30^\circ$ ;  $x_s = 3.81$ ;  $y_s = -0.26$ .

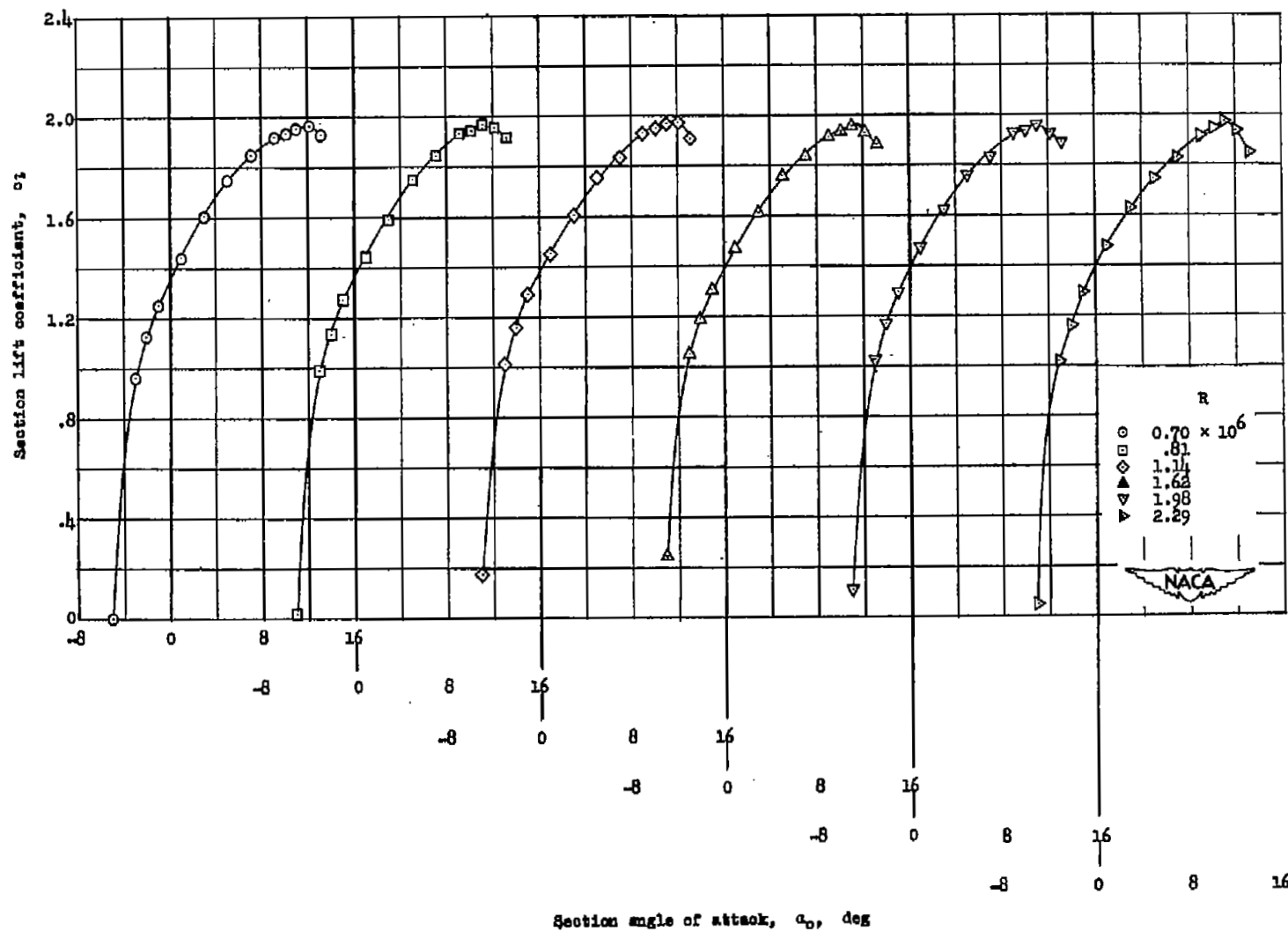


Figure 10.- Section lift characteristics at several values of the Reynolds number for 6-percent-thick symmetrical circular-arc airfoil with drooped-nose flap. Configuration A.

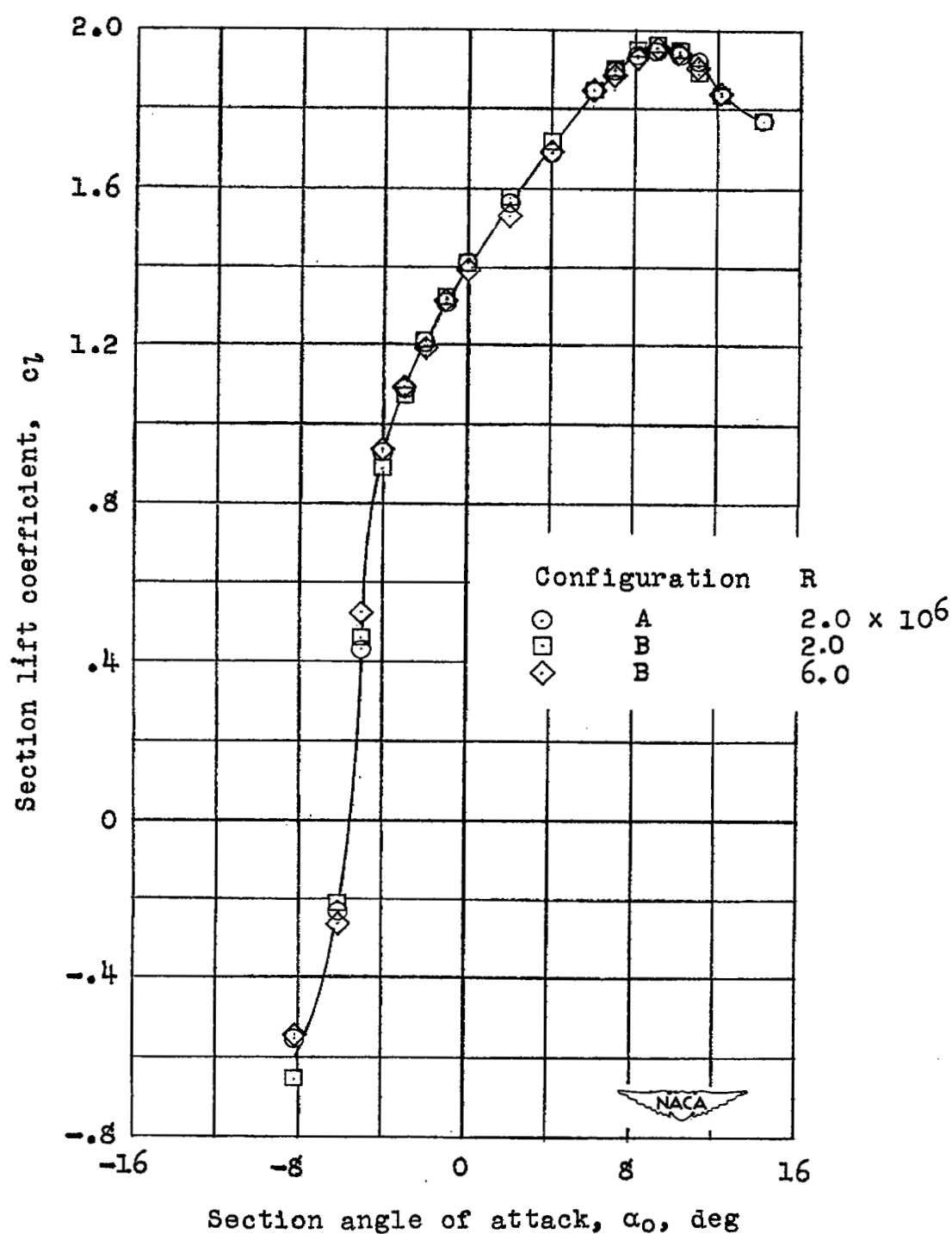


Figure 11.- Section lift characteristics at two values of the Reynolds number for two drooped-nose-flap configurations of 6-percent-thick symmetrical circular-arc airfoil.

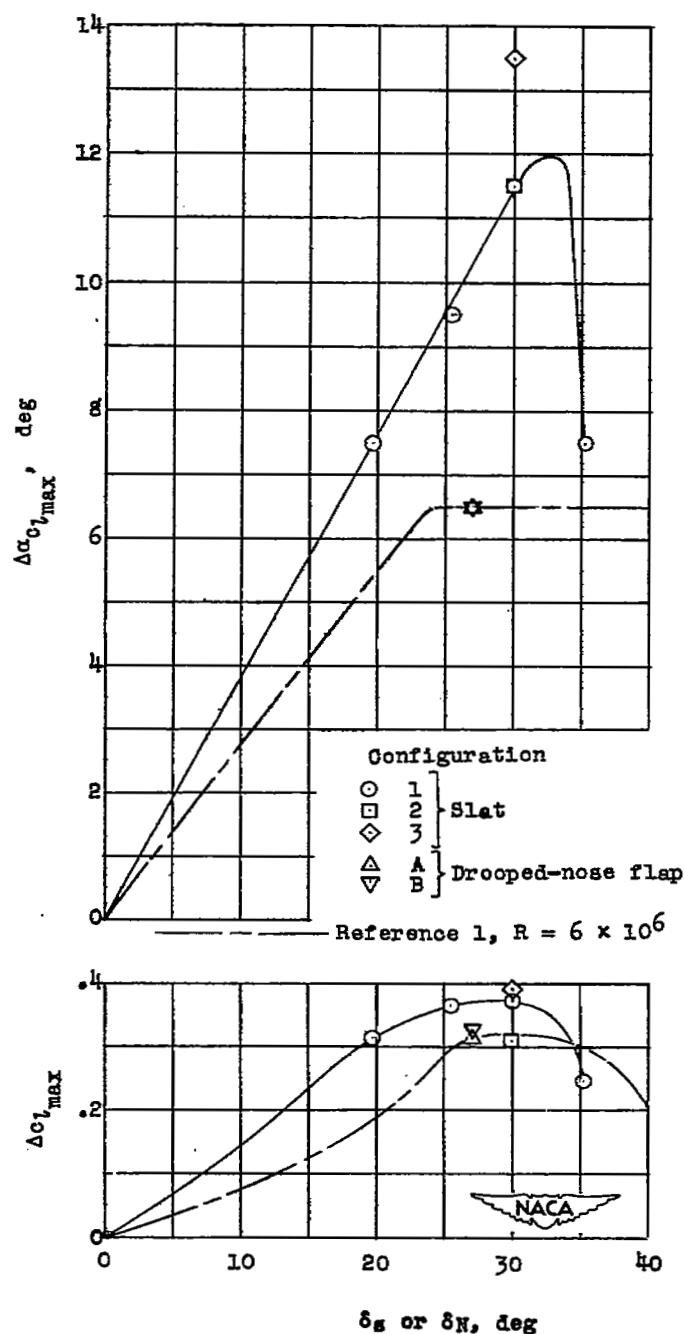


Figure 12.- Variation of the increment in maximum section lift coefficient and the increment in angle of attack for maximum section lift coefficient with deflection of the leading-edge high-lift devices on 6-percent-thick symmetrical circular-arc airfoil.  $R = 2 \times 10^6$ .